EARTH SURFACE PROCESSES AND LANDFORMS
Earth Surf. Process. Landforms (2012)

Published online in Wiley Online Library
(wileyonlinelibrary.com) DOI: 10.1002/esp.3317

Large roughness element effects on sand transport, Oceano Dunes, California

John A. Gillies[1]* and Nicholas Lancaster[2]
[1] Division of Atmospheric Sciences, Desert Research Institute, Reno, NV, USA
[2] Division of Earth and Ecosystems Sciences, Desert Research Institute, Reno, NV, USA

Received 19 August 2011; Revised 31 May 2012; Accepted 19 July 2012

*Correspondence to: John A. Gillies, Division of Atmospheric Sciences, Desert Research Institute, Reno, NV, USA. E-mail: jackg@dri.edu

ESPL
Earth Surface Processes and Landforms

ABSTRACT: The effect of large roughness elements on sand transport efficiency was evaluated on a coastal sand sheet by measuring sand flux with two types of sand traps [Big Spring Number Eight (BSNE) and the Cox Sand Catcher (CSC)] at 30 positions through a 100 m-long × 50 m-wide roughness array comprised of 210 elements each with the dimensions 1·17 m long × 0·4 m high × 0·6 m wide. The 210 elements were used to create a roughness density (λ) of 0·022 ($\lambda = n\,bh/S$, where n is the number of elements, b the element breadth, h the element height, and S is the area of the surface that contains all the elements) in an area of 5000 m^2. The mean normalized saltation flux (NSF) values (NSF = outgoing sand flux/incoming sand flux) at the furthest downwind distance for the two trap types were 0·44 and 0·41, respectively. This is in excellent agreement with an empirical model prediction of 0·5. The reduction in saltation flux is similar to an earlier separate study for an equivalent λ composed of elements of similar height (0·36 m), even though the roughness element forms were different (rectangular in this study as opposed to circular) as were the horizontal porosity of the arrays (49% versus 16%). This corroborates earlier results that roughness element height is a critical parameter that enhances reduction in sand transport by wind for similar λ configurations. The available data suggest the form of the relationship between transport reduction efficiency and height is likely a power relationship with two limiting conditions: (1) for elements ≤ 0·1 m high the effect is minimized, and (2) as element height matches and then exceeds the maximum height of the saltation layer (≥ 1 m), the effect will stabilize near a maximum of NSF ≈ 0·32.

KEYWORDS: sand transport; roughness effects; aeolian processes

Introduction

Roughness elements (e.g. sparse vegetation, large rocks) are known to modulate sand transport by wind. Very sparse roughness can cause increased erosion when the elements are isolated from each other and the individual elements generate a vortex in front and accelerated flow around them (Sutton and McKenna Neuman, 2008), which enhances wind erosion. At a critical density of roughness, entrainment and transport are suppressed due to momentum absorption by the roughness (Gillette and Stockton, 1986; Raupach *et al.*, 1993; Yang and Shao, 2005). The partitioning of shear stress between the elements and the intervening surface reduces the shear stress on the surface (Raupach *et al.*, 1993; Gillies *et al.*, 2007), thus decreasing sand transport as saltation flux scales as a power function of shear stress (Bagnold, 1941). In addition, interaction of the moving sand with the roughness elements, may also affect the transport efficiency (Bagnold, 1941; McKenna Neuman and Nickling, 1994).

Field and wind tunnel data measurements of sand transport through roughness that is on the order of a few centimeters (Al-Awadhi and Willetts, 1999) to tens of centimeters in height (e.g. Lancaster and Baas, 1998; Gillies *et al.*, 2006) have revealed that the reduction in sand transport scales as a power function of the roughness density (λ), which is defined as:

$$\lambda = (nbh)/S \quad (1)$$

where n is the number of elements, b the element breadth, h the element height, S the area of the surface that contains all the elements. According to Yang and Shao (2005), roughness begins to suppress sand transport when $\lambda \geq 0{\cdot}012$.

In addition to the relationship between decreased sand flux with increasing λ, Gillies *et al.* (2006) observed that for similar λ configurations composed of large (0·36 m high) versus small (0·02–0·1 m high) elements the reduction of sand transport was much greater for the taller roughness elements. Gillies *et al.* (2006) suggested that when the dimensions of the roughness elements are equivalent to the full range of saltation length units (i.e. vertical and horizontal saltation path lengths) the increased interaction of elements with the saltation cloud reduces the transport efficiency to a much greater extent than for a surface with smaller roughness elements of equivalent λ. This suggests that λ is an insufficient descriptor of roughness to account for all the observed effects of roughness on sand transport. It has proven to be adequate to characterize shear stress partitioning effects on roughened surfaces over a range of scales and distributions of roughness (e.g. Raupach *et al.*, 2006; Gillies *et al.*, 2007; Brown *et al.*, 2008), but it does not adequately explain roughness element height effects on sediment transport.

The inadequacy of λ to explain how roughness affects transport threshold and the efficiency of sand transport was also addressed by Okin (2008). He developed a model that differs in its approach from Raupach *et al*. (1993), and considers that the distribution and size of open spaces among vegetated roughness, termed gaps, are primarily responsible for affecting the sediment transport system rather than the roughness itself. As it too lacks an explicit roughness element height effect this model may also be unable to account for the observed effect of roughness element height on transport efficiency.

With available data from prior studies it is not possible to define with rigor the nature of the scaling relationship between roughness element height and horizontal sediment flux. This knowledge is critical for modeling how sand transport will be modulated by roughness for terrestrial situations where sand in transport interacts with solid elements or vegetation over a range of height as well as for Martian conditions where sand is transported over surfaces with different concentrations and distributions of large elements (Gillies *et al.*, 2010). In addition, understanding this relationship could improve our ability to use roughness as a means to control sand movement and dust emissions that may accompany the sand movement.

The purpose of this paper is to present new data from a study of sand transport by wind across a coastal sand sheet area that was modified by roughness of similar scale to that used by Gillies *et al*. (2006), and compare the measured dimensionless sand flux through this roughness with dimensionless sand flux and its change as a function of downwind distance observed by Gillies *et al*. (2006). This provides a means to evaluate if the results from both studies are consistent for roughness of similar size, whether the relationship is affected by sediment supply, and how the horizontal porosity (Cornelis and Gabriels, 2005) of the roughness may be affecting the transport efficiency. The data from Gillies *et al*. (2006) represent a supply-limited condition of sediment transport made on a large bare area within the United States Department of Agriculture's (USDA) Jornada Experimental Range, Las Cruces, New Mexico, whereas at the sand sheet site the supply of sand is essentially limitless. In both cases there were no constraints on the boundary-layer flow and saltation system, which in wind tunnel studies of sand transport can create scaling issue concerns due to Reynolds number and Froude number effects (White and Mounla, 1991).

Experimental Procedures

The sediment transport measurements were made in the Oceano Dunes State Vehicular Recreation Area, Oceano, California, in support of a study to evaluate the effectiveness of emplaced roughness to control sand movement and dust emissions. Straw bales were used to modify the surface to create an area with known roughness characteristics as defined by λ (Equation 1) and with controlled dimensions of the roughness itself (Figure 1). There was an approximately 500 m fetch over a smooth sand surface upwind of the established roughness array, providing a well-established boundary-layer with the roughness situated in the atmospheric inertial sub-layer (Wieringa, 1993). Measurements of local winds and sand flux in the established roughness array were conducted from April 15–May 4, 2011.

The straw bales were emplaced on a portion of the sand sheet surface in a staggered array approximately 50 m wide and 100 m long, and the sand transport through the roughness measured using sand traps (Figure 2). The target reduction in sand flux was 50% at the trailing edge of the roughness array. The bale dimensions were 1·17 m long × 0·4 m high × 0·6 m wide. To create a roughness configuration using these bales and achieve

Figure 1. The roughness array at the start of the monitoring period (top panel) and at the end of the monitoring (bottom panel). Dominant winds are from right to left.

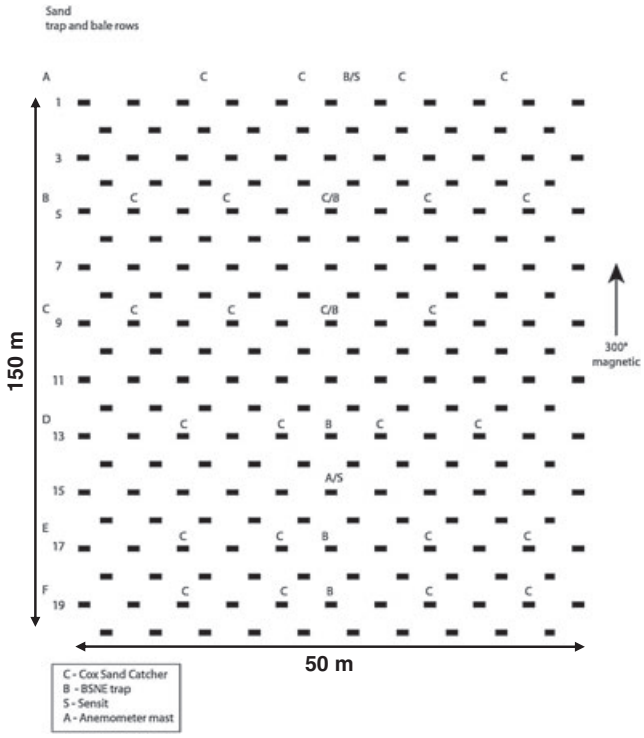

Figure 2. Schematic diagram of the roughness array (not to scale) showing the positions of the sand traps (C and B) and anemometer/wind vane mast (A/S).

the target sand reduction, the relationship between normalized saltation flux (NSF = outgoing sand flux/incoming sand flux) and λ presented by Gillies *et al*. (2006) is:

$$NSF = 0 \cdot 0004\lambda^{-1 \cdot 871} \quad (2)$$

was used to calculate the value of λ that would be required to meet the design criterion (i.e. NSF = 0·5). A value of λ = 0·022 was needed, which required 210 bales be used in the defined area spaced 4·9 m apart, center to center in the lateral dimension and also between rows. The target sand reduction and the bale configuration required to obtain the defined λ were also guided by considerations of logistical constraints imposed by California State Parks (i.e. size of the array and impact on nearby nesting endangered bird species) and cost.

The roughness configuration was established using marked ropes to demarcate the placement of bales across the width of the roughness array and the inter-row distance. An even numbered row of roughness elements consisted of 10 bales and an odd row of 11 (Figure 2). The orientation of the array was set to maximize the frontal area of the bales to the expected dominant wind direction of 300°.

Point measurements of sand flux (kg m^{-2} h^{-1}) were made through the array from upwind of the bales to the trailing edge of the array using two types of sand traps: the Cox Sand Catcher (CSC, Ono *et al.*, 2011) and the Big Spring Number Eight (BSNE, Fryrear, 1986) (see supplementary material). Twenty-four CSCs were placed in six rows of four traps, beginning immediately upwind of the first row of straw bales and then in the center of the lane between straw bale rows 4 and 5; 8 and 9; 12 and 13; 16 and 17; and 18 and 19. BSNEs were installed only in the center of each of the rows at the CSC positions (Figure 2). The height of the inlet for all traps was set at 0·15 m, and adjusted daily to account for changes in sand surface elevation. Sand in the traps was collected on a daily basis. A saltation sensor (Sensit) was co-located with the BSNE trap upwind of the roughness array and a second sensor placed beside a 2·2 m high anemometer/wind direction mast positioned in the center of the array between rows 14 and 15, ≈ 71 m from the leading edge of the roughness (Figure 2) and well past the distance where the shear stress comes into equilibrium with the step change in roughness [i.e. normalized downwind distance (NDD) > 60] (Gillies *et al.*, 2007). Wind speed and direction were sampled every second and compiled into one minute, five minute, and hourly averaged values of wind speed and direction.

Sand flux was calculated using the approach of Ono *et al.* (2011) as follows: the mass of sand collected each day in each BSNE trap and CSC trap was divided by the total time that day that the upwind Sensit was recording sand movement to obtain a transport rate in kg m^{-2} h^{-1}. The upwind Sensit was used because it was not possible to estimate event duration for traps that were not paired with a Sensit. It should be noted that, for the sand transport events studied, the average upwind and within-array Sensit-defined event durations typically differed by less than 5% of the total event duration and were determined to be statistically identical using a *t*-test. For the CSC data the average flux was calculated based on the four traps in each of the six rows. Figure 3 illustrates that there was good correlation between the two trap types, but the CSC trap is less efficient than the BSNE type, however the bias between the two traps due to their different collection efficiencies can be eliminated by using NSF as the measure to compare among traps and measurement locations.

As sand transport was measured at a single height (i.e. 0·15 m) at all the trap locations, the vertically integrated flux could not be calculated with confidence by using, for example, the method of Shao and Raupach (1992) as the rate of change of mass flux with height was not measured. Hence the flux measurements cannot be compared with other studies using absolute values. Although sand flux measurements within the roughness array can be compared in an absolute sense because the mass of sand in each trap was collected at the same sampling height and for the same sampling interval (i.e. the period of time the Sensit registered saltation was occurring), it is more appropriate to normalize these data to allow for comparison of flux rates between the two trap types and at different positions within the roughness array as well as allowing for comparison with other studies. The normalization procedure adopted was to divide each individual measured trap flux rate with the sand flux measured by the traps upwind of the roughness, which we denote as NSF. This allows for comparison of flux data between the two types of traps used in this study as it eliminates errors due to the sampling bias associated with each trap. It also allows for comparison with other studies that measured sand flux in a similar fashion even if the flux rate was based on a vertically integrated sand flux measurement (e.g. Gillies *et al.*, 2006). If there is a consistent relationship between roughness effects for elements of similar height and sand transport rate, the data should collapse into a single relationship regardless of location and sand transport conditions.

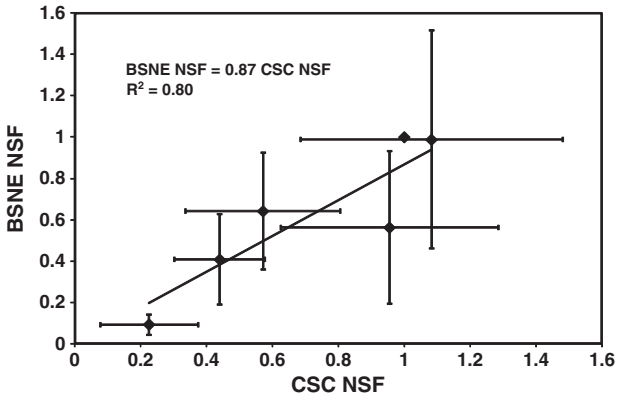

Figure 3. The correlation relationship between the mean Cox Sand Catcher normalized saltation flux (CSC NSF) (mean of six traps per row and 14 transport events) and the mean Big Spring Number Eight normalized saltation flux (BSNE NSF) (mean of single point measurement at each trap location for the 14 transport events).

Results

Sand transport occurred on all days of the study period except April 20 and 23. Very low values of sand transport were measured on April 19, 24, and May 2, and 4. A total of 14 sand transport events lasting several hours or more each provided sufficient amounts of mass in the traps to allow for estimation of the sand flux reduction due to the added straw bale roughness for the two trap types (Table I). The CSC samples collected on April 24 had insufficient mass to process for gravimetric analysis and the BSNE sample of May 1 was lost. The time series of hourly mean wind speed data for the study period is shown in Figure 4. The range of wind speed was 0·3 m s^{-1} to 10·9 m s^{-1} and transport was observed to occur with mean hourly winds in excess of 5·6 m s^{-1} measured at 2·2 m height. On-site wind direction instrumentation failed during the monitoring period, but wind direction observed at the same height (2·2 m) on an adjacent 10 m meteorological tower, located ≈100 m to the south of the study site, and essentially aligned with the middle of the roughness array, showed that transport events only occurred with on-shore winds that were generally perpendicular to the shore. Except for one event (April 21, 2011) with a mean wind direction of 262°, the range of wind direction during transport events was 284° to 306°, which varies only 22° around the expected dominant wind direction of 300°.

Table I. The date, duration, average wind speed and normalized saltation flux (NSF) associated with the 14 sand transport events recorded at the study site

	Event period				NSF near downwind edge	
Date	Start	End	Duration	Average wind speed (m s^{-1})	CSC	BSNE
15 April	12:35	18:00	5:25	6·90	0·19	0·16
16 April	9:55	17:25	7:30	6·91	0·25	0·24
17 April	8:35	17:50	9:15	7·42	0·54	0·80
18 April	11:45	16:20	4:35	5·88	0·55	0·43
21 April	13:00	18:30	5:30	7·26	0·47	0·36
22 April	12:10	16:30	4:20	6·25	0·41	0·35
24 April	12:55	18:25	5:30	6·86	N/A	0·94
25 April	9:50	18:30	8:40	7·20	0·36	0·31
26 April	10:05	18:40	8:35	8·27	0·60	0·56
27 April	9:00	18:45	9:45	7·58	0·51	0·51
28 April	9:15	18:35	9:20	7·97	0·57	0·56
29 April	8:10	17:00	8:50	8·25	0·45	0·39
30 April	10:15	16:55	6:40	5·63	0·53	0·00
1 May	13:20	16:25	3:05	6·43	0·52	N/A
2 May	9:55	16:55	7:00	7·50	0·22	0·07

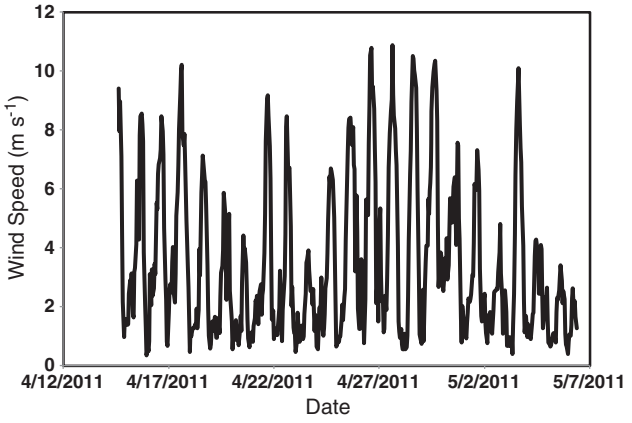

Figure 4. Pattern of wind speeds observed during the study period.

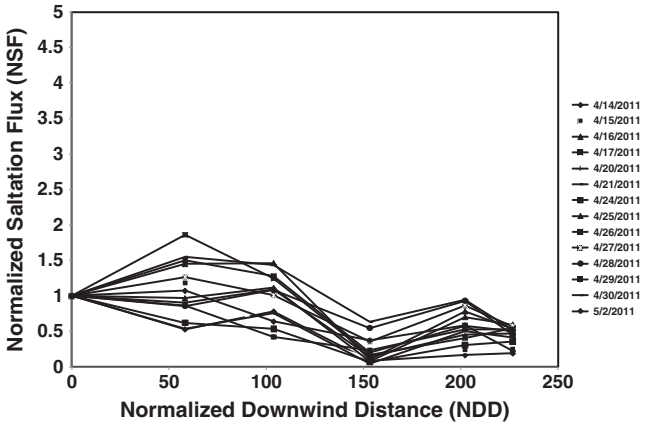

Figure 5. Normalized saltation flux (NSF) as a function of normalized downwind distance as measured with the Cox Sand Catcher (CSC) traps for the 14 sand transport periods.

The effect of the roughness on sand flux through the array of straw bales was assessed by comparing the sand flux measured upwind and sequentially downwind through the array at the designated trap positions. NSF was calculated for each of the traps for the 14 defined transport periods (Table I). The mean NSF near the downwind edge of the array for the CSC and BSNE traps was 0·44 (±0·13) and 0·41 (±0·25), respectively. The numbers in parentheses are the standard deviation of the mean NSF values based on the 14 measured events.

The change in NSF as a function of NDD, where NDD is defined as the horizontal distance from the leading edge of the array divided by the height of the roughness (i.e. 0·4 m), for the CSC and BSNE data are shown in Figures 5 and 6, respectively. As Figures 5 and 6 show, in general, NSF decreases as a function of NDD from the beginning of the array to the end of the roughness. Following the initial decline in NSF, it increases again past NDD = 153, followed by a decrease in NSF at NDD = 202 through to the furthest downwind measurement position in the array (NDD = 227). This pattern of NSF with NDD is due to the presence of a migrating sand wave (approximately 1 m high) in the array, which caused the flow of wind and sand to be disrupted at NDD = 153, due to sheltering effects in its lee. The mean NSF as a function of NDD for the two trap types that does not include the data for NDD = 153 is shown in Figure 7. Least squares regression of these data show that NSF generally decreases exponentially with increasing NDD defined by the relationship: $NSF = 1{\cdot}107e^{(-0{\cdot}004\lambda)}$ with an $R^2 = 0.77$. An exponential decrease

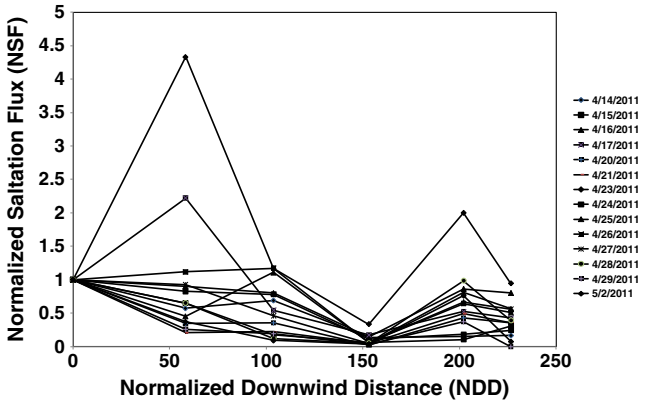

Figure 6. Normalized saltation flux (NSF) as a function of normalized downwind distance as measured with the Big Spring Number Eight (BSNE) traps for the 14 sand transport periods.

in NSF as a function of NDD was also observed by Gillies *et al.* (2006) for their study of sand transport through large scale roughness. The Gillies *et al.* (2006) data for NSF as a function of NDD for their roughness array $\lambda = 0{\cdot}03$ are also shown for comparison purposes in Figure 7.

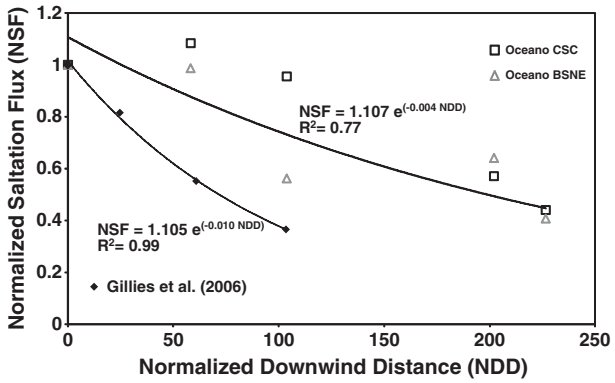

Figure 7. Normalized mean saltation flux (NSF) as a function of normalized downwind distance (NDD) for both trap types. Regression-derived relationship uses combined Oceano CSC and BSNE data. The Gillies *et al.* (2006) data are from for their $\lambda = 0{\cdot}03$ roughness array, but the data have been re-plotted to start at NDD = 0, whereas in Gillies *et al.* (2006) the first measurement was upwind of their array at NDD = –14·6.

Discussion

The mean NSF values at the trailing edge of the roughness array are compared with the data of NSF as a function of λ presented by Gillies *et al.* (2006) in Figure 8. The Oceano data sit close to the relationship developed by Gillies *et al.* (2006), i.e. Equation 2, but the mean values of NSF based on data from the two trap types (i.e. 0.44 and 0.41) for λ = 0.022 are lower than the predicted value of 0.5, but lie within the 95% confidence interval of the NSF versus λ relationship defined by Equation 2. The greater reduction in transport for the straw bales versus the roughness used by Gillies *et al.* (2006) (i.e. five gallon plastic buckets) may be due to the bales being slightly taller than the buckets (0·4 m versus 0·36 m). The scaling of transport efficiency as a function of element height may be a result of several mutually reinforcing factors, including the physical interaction of the saltating particles with the roughness elements in the vertical and horizontal directions, the storage of sediment in the lee of the roughness, and the effect the roughness has on the saltation cloud energetics.

As suggested by Gillies *et al.* (2006), as the ratio of saltation cloud height to roughness element height approaches one, there is an increased potential for reducing transport efficiency because a greater percentage of the particles in motion have a higher probability of being intersected in their trajectories by the taller roughness (Figure 9). Nield and Wiggs (2011) observed that saltation cloud heights reached 0·7 m on a beach in Wales using terrestrial laser scanning (TLS). Other published data from large wind tunnels (height > 0·5 m) (e.g. McKenna Neuman and Nickling, 1995) also indicate saltation on sand surfaces rises to heights in excess of 0·5 m. As roughness protrudes higher into the saltation cloud it can remove (by impact with the roughness) those particles that reach higher horizontal speeds. Removing the higher speed particles also removes the particles that upon impact splash up a great number of particles than slower moving particles. The number of particles that splash up from the impact of a saltating particle impacting the surface is linearly proportional to their momentum (Kok and Renno, 2009). Reduction in the momentum of saltating particles would therefore reduce the mobilization of particles in the open area among the roughness elements and hence the flux. Roughness, and especially higher roughness, therefore acts to capture higher energy saltating grains thus removing their potential to recruit more particles into the saltation cloud via the splash effect hence lowering the flux of particles in transport.

Anderson (1986), using the saltation model of Anderson and Hallet (1986), calculated the vertical kinetic energy flux of saltating (and suspended) particles and observed that the kinetic energy flux reached a maxima above the surface at a height which scales as a function of shear velocity (u_*) and particle size. For a high wind shear condition ($u_* = 1{\cdot}0$ m s^{-1}) transporting a distribution of particle sizes, the kinetic energy flux maxima as shown by field evidence and Anderson's (1986) model occurs between 0·1 m and 0·4 m, depending on the hardness of the surface (Figure 9). If roughness elements interfere with this zone of highest kinetic energy, this should remove a proportionally higher amount of kinetic energy flux with the result being that less energy is available throughout the saltation cloud, which should reduce the mass flux of saltating particles. This could be tested empirically, but is beyond the scope of the present paper.

A second factor related to the physical interaction of particles in motion with the roughness that could affect the efficiency of the bales to reduce sand transport as compared to the buckets

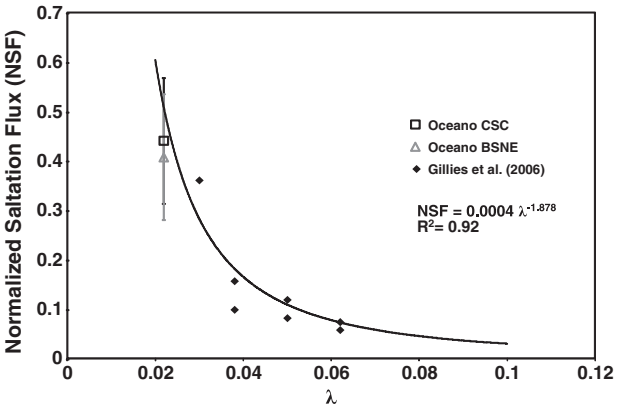

Figure 8. Normalized mean saltation flux (NSF) as a function of λ including data from both trap types at Oceano and the data from Gillies *et al.* (2006). The regression-derived relationship is for all data combined. Error bars on the Oceano data points represent the standard deviation of the mean.

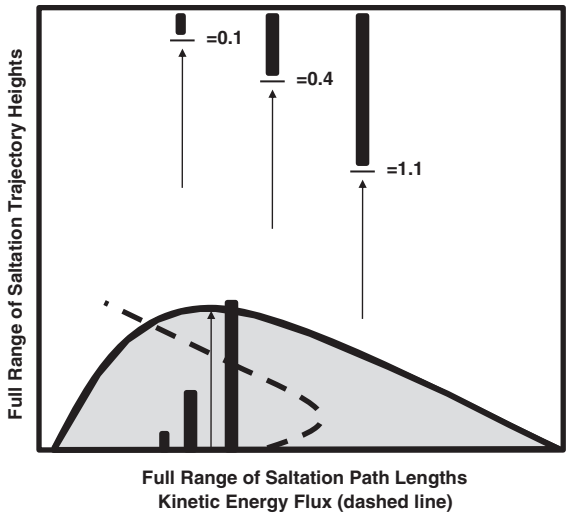

Figure 9. Schematic diagram showing idealized length scale relationships between roughness element height and the full range of saltation path lengths (vertical and horizontal) indicated by the shaded area. The ratio of element height to the full range of the vertical depth of the saltation cloud is presented diagrammatically in the top half of the panel. The relationship between element height and the vertical kinetic energy flux profile (dashed line) in the saltation cloud as presented by Anderson (1986) is also shown for a shear velocity of 1 m s^{-1}.

used by Gillies *et al*. (2006) is the horizontal dimension of the roughness with respect to the size of the gap between elements, i.e. the horizontal porosities of the two roughness arrays. Horizontal porosity is defined by Cornelis and Gabriels (2005) as the open cross-sectional area divided by the total cross-sectional area. For the staggered array form of roughness the open cross-sectional area is defined as the total cross-sectional area (i.e. array width × element height) minus the sum of all element frontal areas in two sequential rows. For the roughness emplaced at Oceano Dunes the horizontal porosity is 0·49, while for the least dense array tested by Gillies *et al*. (2006), i.e. $\lambda = 0{\cdot}03$, the associated horizontal porosity was 0·16 (a factor of three lower compared to Oceano). The greater interaction of the sand with the roughness elements in the lateral dimension for the case of the Oceano Dunes roughness may have also contributed to the lower mean NSF value for the bales versus the buckets. Mean NSF values for Oceano are between 12–18% lower than the empirical model-predicted values, but the horizontal porosity is approximately three times greater at Oceano than Jornada, suggesting that element height has a greater effect on transport efficiency than horizontal porosity.

As Figure 7 shows, an exponential decrease in NSF as a function of NDD was observed in this study and in the Gillies *et al*. (2006) study. As Gillies *et al*. (2006) showed (see figure 5 in that paper) the rate of change of NSF with NDD also scales with λ, increasing at a greater rate as λ increases, and it is not related to shear stress partitioning effects as the adjustment of shear stress to the step change in roughness is complete at ≈NDD = 60 (Gillies *et al*., 2006). According to Gillies *et al*. (2006), the rate of change is defined by the *b* coefficient in the general relationship: $\mathrm{NSF} = a\, e^{(b \times \mathrm{NDD})}$ and when this coefficient is plotted as a function of λ a predictive relationship is observed. The relationship for their four different λ configurations is:

$$b = 0 \cdot 019 \ln\lambda + 0 \cdot 0758 \tag{3}$$

Based on this relationship the *b* exponent for the Oceano Dune NSF versus NDD relationship should be 0·0046. The value of the *b* exponent for the Oceano Dunes relationship (Figure 7) is 0·004, suggesting that this relationship is applicable across a wider range of λ and that sediment supply does not have much of an effect. Combining the data from this study with those of Gillies *et al*. (2006), the relationship between the *b* coefficient and λ improves the correlation coefficient of the general relationship to 0·97 from 0·94, as reported by Gillies *et al*. (2006) (Figure 10).

With the collection of the Oceano data there is now a limited data set available to provide an evaluation of the height effect on transport efficiency for large versus small roughness elements for surfaces of the same λ value. Using the NSF versus λ data presented in Gillies *et al*. (2006) (their figure 7) and the Oceano data, the element height effect on transport efficiency can be demonstrated. For λ = 0·022, the NSF and λ relationship for the Al-Awadhi and Willetts (1999) (average element height = 0·035 m) and Lancaster and Baas (1998) (average element height = 0·1 m) data sets, would predict essentially no measureable effect of element height on sand transport efficiency. For the Gillies *et al*. (2006) study (element height = 0·36 m) and λ = 0·022, NSF = 0 50, and for the Oceano data (element height = 0·4 m) the mean NSF is 0·43. These data are plotted in Figure 11A and show the trend of the expected relationship of increasing element height and decreasing transport efficiency. The actual form of the relationship, linear or power function, remains to be determined but Figure 11A provides a first approximation for characterizing the height effect. A model of the general relationship between roughness element height and NSF, for the available λ = 0·022 data is presented in Figure 11B, which shows element height has no effect on transport efficiency below $h = 0{\cdot}1$ m, then a non-linear effect between 0·1 m and h = 1 m (an assumed maximum

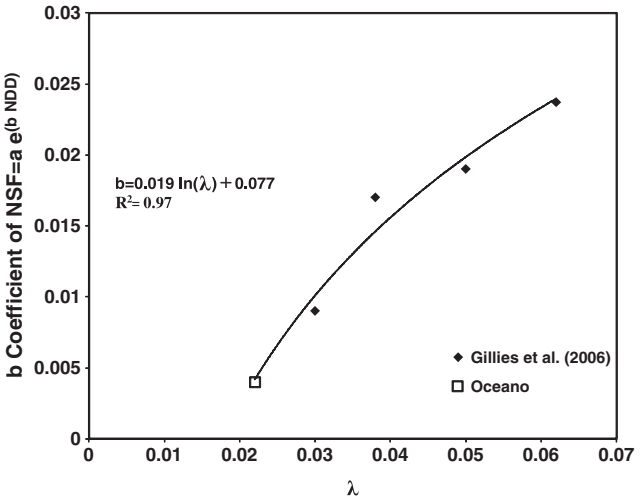

Figure 10. The relationship between the *b* coefficient in the $\mathrm{NSF} = a\, e^{(b \times \mathrm{NDD})}$ relationship and λ for the Oceano data and the data from Gillies *et al*. (2006) showing the Oceano data fit the expected pattern. The regression-derived relationship combines all the data.

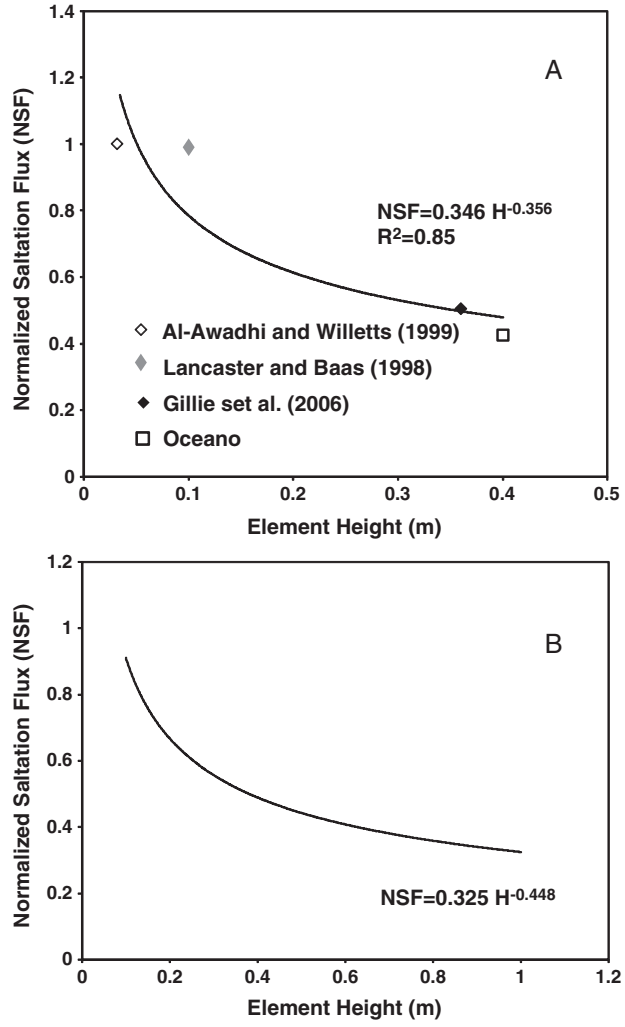

Figure 11. (A) The relationship between NSF and element height for λ = 0·022 arrays based on available data from this study, Al-Awadhi and Willetts (1999), Lancaster and Baas (1998), and Gillies *et al*. (2006). (B) the generalized relationship between NSF and element height for λ = 0·022 for element height between 0·035 m and 1 m.

saltation cloud height). For surfaces with roughness elements that extend above the maximum height of the saltation layer, no further physical interaction will take place, leaving perhaps only additional aerodynamic effects to modulate the sediment transport process through shear stress partitioning effects.

The physics of how roughness element height affects the efficiency of sand transport for similar λ values remains to be resolved. From the available data it appears to be related to the ratio of element height to saltation layer height, but this by itself does not provide a causal mechanism. It will require much more detailed measurements of the interaction of the saltation layer with the roughness and the boundary-layer to determine explicitly whether it is the physical interaction of the particles in transport with the roughness, the interruption of the kinetic energy flux, shear stress partitioning effects, trapping of particles in the lee of roughness, or a combination of these effects to explain exactly how the roughness diminishes the sediment flux due to an increase in element height.

Conclusions

The collection of a new data set of sand flux measurements through a roughness array composed of large elements lying on a sand sheet in the atmospheric inertial sub-layer allowed for the comparison with results from a similar study (Gillies *et al.*, 2006), but with several key differences. For similar roughness densities, 0·022 for this study and 0·030 for the study by Gillies *et al.* (2006), there were differences in the actual size and form of the roughness elements and the sediment supply conditions. The difference in the form of the roughness between the two studies is that the Oceano roughness elements were rectangular in nature while the elements used by Gillies *et al.* (2006, 2007) were circular, with the projected frontal area having the form of an isosceles trapezoid. The study of Gillies *et al.* (2006) was carried out under restricted sand supply while for this study sediment supply was unrestricted, limited only by the transport capacity of the wind. Despite the differences in element form and sediment supply the data from each of the studies is complimentary and corroborative. The sand flux data, as characterized by the NSF values at the downwind edges of the roughness for both studies, demonstrates that the reduction in flux scales as power function of λ, and critically, the newly-available data match the results of Gillies *et al.* (2006) showing that large roughness elements are more effective at reducing sand flux than smaller elements for equivalent λ. The combined data from the two studies suggest that between elements 0·03 m to 0·1 m high and elements around 0·38 m high, the NSF would change from 1 to ≈0·48 due to the height effect. The exact nature of the relationship between the two height ranges that represent the entire available data set remains to be determined. Logic suggests the form of the relationship between transport reduction efficiency and height is likely a power relationship with two limiting conditions (Figure 11A). For elements ≤ 0·1 m high the effect is minimized. As element height matches and then exceeds the maximum height of the saltation layer (≥ 1 m), the effect will stabilize near a minimum of NSF of ≈0·32 (Figure 11B). It should be noted that this is based on only one λ measurement (0·022). Additional scaling effects may be present as λ increases above this value, but these remain unknown. The effect of roughness element distribution and size however, must be incorporated into wind-blown transport models if they are to produce reasonable results. This and other published work indicates that sediment transport rates scale predictably with changes in λ, however, this non-dimensional parameter of roughness is insufficient to account for all observed effects and it remains a research challenge to develop a parameter (or parameters) for roughness that can account for both the scale independent and scale dependent effects of roughness on aeolian sediment transport.

Despite its limitations, λ can still be used effectively to guide engineered approaches to controlling sand transport. The data presented in this paper, combined with the results of Gillies *et al.* (2006), demonstrate that the rate of change in the sand transport efficiency as a function of NDD scales with λ in a predictable fashion over the range λ = 0·022–0·062, for elements in the size range tested (i.e. ≈0·035 m to ≈0·4 m, Figure 10). This information could prove to be very practicable when using roughness for controlling sand movement. For example, having a higher λ or elements of greater height at the leading edge of a roughness array could be very beneficial for quickly reducing the transport efficiency that could be followed by a lower λ configuration, thus saving resources, but one designed to some critical criterion. It may be more efficient to manage the leading edge of the array by, for example, removing built up sediment there instead of larger scale maintenance to manage the entire roughness array.

Acknowledgments—This work was supported by a contract between the Desert Research Institute and California State Parks and the San Luis Obispo County Air Pollution Control District (SLOCAPCD), San Luis Obispo, California. The authors would also like to acknowledge Ronnie Glick (California State Parks), Gary Willey and Larry Allen (SLOCAPCD) for their personal contributions to the study and the support of their respective institutions to facilitate the required permitting. The authors would also like to thank the personnel from both institutions who aided in the installation and maintenance of the field experiment for their efforts.

Supporting Information

Supporting information may be found in the online version of this article.

References

Al-Awadhi JM, Willetts BB. 1999. Sand transport and deposition within arrays of non-erodible cylindrical elements. *Earth Surface Processes and Landforms* **24**: 423–435.

Anderson RS. 1986. Erosion profiles due to particles entrained by wind: application of an eolian sediment-transport model. *Geological Society of America Bulletin* **97**: 1270–1278.

Anderson RS, Hallet B. 1986. Sediment transport by wind: toward a general model. *Geological Society of America Bulletin* **97**: 523–535.

Bagnold RA. 1941. *The Physics of Blown Sand and Desert Dunes*. Chapman and Hall: London.

Brown S, Nickling WG, Gillies JA. 2008. A wind tunnel examination of shear stress partitioning for an assortment of surface roughness distributions. *Journal of Geophysical Research – Earth Surface* **113**: F02S06. DOI. 10.1029/2007JF000790

Cornelis WM, Gabriels D. 2005. Optimal windbreak design for wind erosion control. *Journal of Arid Environments* **61**: 315–332.

Fryrear DW. 1986. A field dust sampler. *Journal of Soil and Water Conservation* **41**: 117–120.

Gillette DA, Stockton PH. 1986. Mass momentum and kinetic energy fluxes of saltating particles. In *Aeolian Geomorphology*, Nickling WG (ed.). Allen and Unwin: Boston, MA; 35–56.

Gillies JA, Nickling WG, King J. 2006. Aeolian sediment transport through large patches of roughness in the atmospheric inertial sublayer. *Journal of Geophysical Research – Earth Surface* **111**: F02006. DOI. 10.1029/2005JF000434

Gillies JA, Nickling WG, King J. 2007. Shear stress partitioning in large patches of roughness in the atmospheric inertial sublayer. *Boundary-Layer Meteorology* **122**: 367–396. DOI. 10.1007/s10546-006-9101-5

Gillies JA, Nickling WG, King J, Lancaster N. 2010. Modeling aeolian sediment transport thresholds on physically rough Martian surfaces: a shear stress partitioning approach. *Geomorphology* **121**: 15–21. DOI. 10.1016/j.geomorph.2009.1002.1016

Kok JF, Renno NO. 2009. A comprehensive numerical model of steady state saltation (COMSALT). *Journal of Geophysical Research-Atmospheres* **114**: D177204. DOI. 10.1029/2009JD011702

Lancaster N, Baas A. 1998. Influence of vegetation cover on sand transport by wind: field studies at Owens Lake California. *Earth Surface Processes and Landforms* **25**: 68–82.

McKenna Neuman CK, Nickling WG. 1994. Momentum extraction with saltation: implications for experimental evaluation of wind profile parameters. *Boundary-Layer Meteorology* **68**: 35–50.

McKenna Neuman C, Nickling WG. 1995. Aeolian sediment flux decay: non-linear behaviour on developing deflation lag surfaces. *Earth Surface Processes and Landforms* **20**: 423–435.

Nield JM, Wiggs GFS. 2011. The application of terrestrial laser scanning to aeolian saltation cloud measurement and its response to changing surface moisture. *Earth Surface Processes and Landforms* **36**: 273–278.

Okin GS. 2008. A new model of wind erosion in the presence of vegetation. *Journal of Geophysical Research – Earth Surface* **113**: F02S10. DOI. 10.1029/2007JF000758

Ono D, Kiddoo P, Howard C, Davis G, Richmond K. 2011. Application of a combined measurement and modeling method to quantify windblown dust emissions from the exposed playa at Mono Lake, California. *Journal of the Air & Waste Management Association* **61**(10): 1036–1045.

Raupach MR, Gillette DA, Leys JF. 1993. The effect of roughness elements on wind erosion threshold. *Journal of Geophysical Research* **98**: 3023–3029.

Raupach MR, Hughes DE, Cleugh HA. 2006. Momentum absorption in rough-wall boundary layers with sparse roughness elements in random and clustered distributions. *Boundary-Layer Meteorology* **120**: 201–218. DOI. 210.1007/s10546-10006-19058-10544

Shao Y, Raupach MR. 1992. The overshoot and equilibration of saltation. *Journal of Geophysical Research-Atmospheres* **97**: 20559–20564. DOI. 10.1029/92JD02011

Sutton SLF, McKenna Neuman C. 2008. Sediment entrainment to the lee of roughness elements: effects of vortical structures. *Journal of Geophysical Research – Earth Surface* **113**: F02S09. DOI. 10.1029/2007JF000783

White BR, Mounla H. 1991. An experimental study of Froude number effect on wind-tunnel saltation. *Acta Mechanica Suppl.* **1**: 145–157.

Wieringa J. 1993. Representative roughness parameters for homogeneous terrain. *Boundary-Layer Meteorology* **63**: 323–363.

Yang Y, Shao Y. 2005. Drag partition and its possible implications for dust emission. *Water, Air, and Soil Pollution: Focus* **5**: 251–259.